Available online at www.sciencerepository.org

Science Repository

Research Article

Autologous Adipose-Derived Stem Cells, Platelet-Rich Plasma, and Fibrin Enhance Healing of Mandibular Bone Defects in Swine

Aaron J. Maki[1], Rathnaweera A.C. Rabel[1,6], Marcello Rubessa[1], Anna C. Ercolin[1,5], Kelly S. Roballo[1,5], Jamey J. Cooper[1] and Matthew B. Wheeler[1,2,3,4*]

[1]*Department of Animal Sciences, University of Illinois at Urbana-Champaign, Urbana, Illinois, USA*
[2]*Carl R. Woese Institute for Genomic Biology, University of Illinois at Urbana-Champaign, Urbana, Illinois, USA*
[3]*Department of Bioengineerring, University of Illinois at Urbana-Champaign, Urbana, Illinois, USA*
[4]*Department of Biomedical and Translational Sciences, Carle-Illinois College of Medicine, University of Illinois at Urbana-Champaign, Urbana, Illinois, USA*
[5]*Department of Veterinary Medicine, University of Sao Paulo, Pirassununga, Brazil*
[6]*Department of Farm Animal Production and Health, Faculty of Veterinary Medicine and Animal Science, University of Peradeniya, Peradeniya, Sri Lanka*

ARTICLE INFO

Article history:
Received: 27 May, 2020
Accepted: 10 June, 2020
Published: 18 June, 2020

Keywords:
ASC
bone regeneration
fibrin
platelet-rich plasma
mandible
porcine

ABSTRACT

The primary aim of this study was to assess the therapeutic effects of autologous platelet-rich plasma and fibrin scaffolds combined with autologous adipose stem cells (ASCs) for critical-size defects in the pig mandible. Fibrin scaffolds supplemented with calcium hydrogen phosphate and platelet-derived growth factors were hypothesized to accelerate healing in porcine mandible bone compared to ASC-only injections and untreated controls. Three treatments included the use of autologous ASCs from liposuction with the addition of platelet-rich plasma, fibrin scaffolds, or as cell-only controls. All three treatments using ASCs were determined to increase bone mineral density and bone volume fraction compared to untreated controls. In general, the addition of both platelet-rich plasma and fibrin scaffolds to autologous ASCs from liposuction improved bone healing of critical-size defects.

Introduction

Delayed or non-union bone defects do not heal spontaneously without clinical intervention and are the result of numerous clinical conditions, including tumor resections, congenital abnormalities, and traumatic injuries [1, 2]. About 500,000 patients in the United States are affected annually, an estimated 5-10% of all bone fractures [3, 4]. Tissue engineering and regenerative medicine focus on improving the healing of the patients. Specifically, in the area of bone healing/regeneration, the goal is the interaction with host tissues to stimulate regeneration and reduce the formation of scar tissue [5]. The "gold standard" for bone healing is still the autologous bone, with all its pros and cons [6, 7]. The newly regenerated bone would retain its ability to repair and remodel itself over the patient's lifetime, potentially achieving similar levels of integration as an autograft without requiring the inconvenient second surgical site. The tissue engineering triad involves the use of scaffolds, growth factors, and cells [8]. Scaffolds provide an intermediate surface for cells to attach and guide the process of tissue formation. Over time,

Correspondence to: Matthew B. Wheeler, Ph.D., Professor of Biotechnology and Developmental Biology, Department of Animal Sciences, Carl R. Woese Institute for Genomic Biology, Department of Bioengineering, Department of Biomedical and Translational Sciences, University of Illinois, 1207 West Gregory Drive, Urbana, Illinois 61801, USA; Fax: 2173338286; Tel: 2173332239; E-mail: mbwheele@illinois.edu

http://dx.doi.org/10.31487/j.RGM.2020.02.01

these scaffolds are resorbed to make space for newly forming tissue. Growth factors provide instructions for migration, proliferation, and differentiation of cells to form bone and other important support structures such as vascular networks. The sources of these essential elements are important in determining the outcome of any proposed therapy.

Currently, most tissue engineering strategies utilize synthetic scaffolds, recombinant growth factors, and/or culture-expanded stem cells. While both autografts and tissue engineering are the future of bone defect repair, it is possible that a hybrid, autologous tissue engineering approach, where cells, scaffolds, and growth factors are acquired from the patient, may capitalize on the advantages of each technique. An autologous tissue engineering method, as detailed in this research, has the potential to maintain similar performance and compatibility to an autograft without requiring harvesting of patient bone, thus avoiding associated complications. Blood may present an alternative source of autologous materials for use in craniofacial bone defect repair. Compared to the bone, blood is more accessible, more plentiful in supply, and results in less structural deformity following collection.

Therapeutically, clotted blood and its derivatives, such as fibrin glue and fibrin sealant, have been recognized for their useful properties of hemostasis and tissue adhesion since the 1980s and have been widely used to reduce blood loss during and bleeding after surgical procedures [9-11]. Fibrin sealants can also be utilized as carriers for the release of drugs, such as growth factors and antibiotics, due to their biocompatibility and resorption in a matter of weeks. Past advances in the isolation, characterization, and differentiation of relatively rare adult stem cell populations have opened up new opportunities for the treatment of a wide range of clinical conditions. Due to their properties of promoting vascularization, modulating inflammation, and promoting tissue formation, adipose-derived stem cells (ASCs) have been investigated for treating muscular dystrophy, diabetes, autoimmune disorders, and graft versus host disease, among others [9, 12-15].

While precise mechanisms of action for ASC healing of bone defects are unknown, vascular infusion or direct injection of undifferentiated ASCs have the potential to remedy critical-size bone defects by migration, proliferation, and differentiation into the proper cell types required by the regenerating tissue. Other effects include their generally anti-inflammatory cytokine release profile and recruitment of surrounding cells by secretion of growth factors and cytokines [16]. At the site of a bone defect, ASCs may modulate the inflammatory response, recruit surrounding cells, and/or differentiate into osteoblasts to directly build new bone. The primary aim of this study was to assess the therapeutic effects of autologous platelet-rich plasma (PRP) and fibrin scaffolds combined with autologous ASCs for critical-size defects in the pig mandible. An autologous tissue engineering approach utilizing ASCs from lipoaspirate may improve the healing outcomes of critical-size bone defects. Combining blood-derived growth factors and fibrin scaffolds with adult stem cells derived from fat comprises an autologous tissue engineering construct, which may result in further improvements in bone healing.

We chose the pig as the animal model for the similarity with humans: bone morphology, anatomy, and the comparable healing and remodeling process [17-19].

Materials and Methods

I Liposuction

The University of Illinois Institutional Animal Care and Use Committee approved all of the following procedures (IACUC #10014). Twelve female Yorkshire pigs (Sus scrofa domesticus) aged 1-3 years and weighing 170-275 kg were included in the study. For ASC extraction, liposuction was performed using standard protocols [20]. Following general anesthesia (5% Isoflurane, Baxter, Deerfield, IL) and sufficient skin sterilization with Betadine (Butler Animal Health, Dublin, OH), 70% ethanol, and zephiran chloride (Winthrop Laboratories, New York, NY), pinpoint incisions were made at 4-6 locations on either side of the dorsal midline using a trocar. Sterile 0.9% saline (Vedco, St. Joseph, MO) with epinephrine (1 mg/L, IMS Limited, El Monte, CA) was injected into subcutaneous adipose deposition sites using a 60 mL syringe connected to a Cobra cannula (3 mm diameter, 25 cm length, Shippert Medical, Centennial, CO). Approximately 10-20 mL of saline was infused per injection and allowed to remain several minutes before collection to promote vasoconstriction and reduce blood loss. A liposuction cannula (Triport, 4 mm diameter, 15 cm length, Shippert Medical) connected to a suction pump (75 kPa, Schuco Inc., Indianapolis, IN) was inserted to collect the lipoaspirate (300-400 mL total). Liposuction time was 60-75 minutes.

II Isolation of Adipose-Derived Stem Cells

Collected lipoaspirate was added to 250 mL centrifuge tubes (Corning Inc., Corning, NY) and mixed on a shaker plate with an equal volume of type I collagenase (0.075%, Sigma C2674) for 60 minutes at 37°C to digest extracellular matrix [15, 21]. The mixture was centrifuged for 10 minutes at 1400 rpm (547 X g) to separate low-density adipocytes from the higher-density stromal vascular cell fraction, which contains ASCs along with other additional cell types, such as fibroblasts, endothelial cells, and smooth muscle cells. The remaining cell pellet was removed and placed in 50 mL conical tubes to be centrifuged for 5 minutes at 1400 rpm (547 X g). Two (2) mL of red blood cell lysis buffer (Sigma R7757, St. Louis, MO) was added to the pellet for 2 minutes, then diluted with PBS (Sigma D5773) and centrifuged for 5 minutes at 1400 rpm (547 X g). The isolation of ASCs was repeated 1-2 times to remove red blood cells. The final pellet was mixed with serum-free DMEM (Sigma D5648) and filtered with a 100 μm cell strainer (Fisher Scientific, Fair Lawn, NJ). Cells collected were split into two syringes, each having a volume of 5 mL. The total processing time for isolation of ASCs was 120-150 minutes. Following 10% formalin (Fisher Scientific) fixation after 5 and 60 minutes, the number of nucleated cells was estimated using DAPI (Sigma D9542) staining and hemocytometer counting. A tracer amount (1 million) of GFP-ASCs was added to the cell injections of 3 pigs to analyse cell engraftment.

III Surgical Procedures

Following the completion of liposuction, pigs were placed in a supine position with sufficient padding. Lower jaws were shaved and sterilized before placing iodine (Ioban, 3M, St. Paul, MN) and thyroid drapes (Kimberly Clark, Roswell, GA). The initial approach through the skin was made by a scalpel and followed up by electrocautery pencil (ConMed, Utica, NY) through fat and muscle. The periosteum was

moved by the periosteal elevator. Transcortical osteotomies, 25 mm in diameter, were performed on the posterior region of the mandible (ramus) using a trephine (Irwin Tools, Huntersville, NC) and a power drill (Milwaukee Tools, Brookfield, WI) with adequate irrigation [14, 22]. One surgical defect was created on each side of the ramus of the mandible (two total per pig). Removed bone cylinders were stored at -20ºC for later analysis.

Following removal of bone, the periosteum was sutured to form a pouch with 2-0 or 3-0 polyglactin resorbable suture (Vicryl, Ethicon, Somerville, NJ). Treatments (5 mL volume) were injected into the defect, and the periosteum was closed. Muscle, fat, and skin layers were then sutured continuously, and the wound was sealed with cyanoacrylate skin glue (Vetbond, 3M, St. Paul, MN). Pigs were administered an analgesic (Banamine, Purdue Products, Somerville, CT) and antibiotic (Excede, Pfizer, New York, NY) and allowed to recover. Pigs were maintained on a soft diet for 1-3 days post-surgery and then resumed standard feed.

IV Blood Extraction and Processing

Blood draws were used to acquire the fibrin scaffolds and PRP. For PRP, 8.5 mL of blood was collected from the ear vein using a 21 gauge butterfly needle (Jorgenson, Loveland, CO) and a 10 mL syringe filled with 1.5 mL of 3.3% sodium citrate. Anticoagulated blood was transferred to 15 mL centrifuge tubes. Initial centrifugation was performed at 1800 rpm (905 X g) for 15 minutes for the removal of RBCs and the collection of plasma. A subsequent spin of collected plasma at 3000 rpm (2510 X g) for 10 minutes separated platelets [23]. A total volume of 2-3 mL of PRP was collected for injection (1-1.5 mL per defect). Before injection, PRP was combined with cell/DMEM mixture (20% PRP concentration) and 50 µL of 10% calcium chloride for platelet activation. Cell-PRP mixture was then injected, and the periosteum closed.

For fibrin scaffolds using whole blood, pigs were placed in a laterally recumbent position for each defect. 3-5 mL of blood was collected from the ear vein in a 10 mL syringe already containing 1 mL of cell/DMEM mixture and then quickly injected into the defect while still in the liquid phase. Calcium hydrogen phosphate (0.1 mL of 0.3 M) was added and stirred in the defect.

V Computed Tomography

Eight weeks post-surgery, pigs were humanely euthanized and the mandibles were collected for analysis of bone healing. Four freshly harvested whole mandibles were scanned using computed tomography (GE Medical Systems, Waukesha, WI) at the University of Illinois Veterinary Medicine Teaching Hospital. Scanning parameters were 120 kV and 64 mA. Three-dimensional images were analysed for gross anatomical information (Carestream, Rochester, NY).

VI Dual Energy X-ray Absorptiometry

Following the removal of soft tissue, samples were scanned using DXA (Hologic QDR 4500A, Bedford, MA) to measure bone mineral density (BMD). Two X-ray beams with different energy levels are passed through the bone, and intensities are measured for each beam. Intensity varies depending on the thickness of the bone and the amount of calcification. Based on the difference between the two beams, BMD was estimated [24]. The original bone removed during the surgery served as a control for comparison and was scanned alongside the defect. Relative change in BMD was calculated as BMD of the defect divided by BMD of the original bone removed during surgery.

VII Micro-Computed Tomography

Samples were trimmed with a band saw and were scanned using microCT (Skyscan 1172, Kontich, Belgium) to determine the degree and location of bone defect healing [22, 25, 26]. MicroCT utilizes the variable X-ray attenuations of different materials to image samples. X-rays pass through the sample form a 2-D projection image. The sample was then slowly rotated, allowing the capture and output of a series of images. The scanner was operated at 75 kV and 100 mA with a 1mm aluminum filter to reduce low energy noise. The medium resolution setting at 95% camera gain was utilized so that projection images were taken at 0.4 degree increments over a range of 180 degrees. A frame average of five projection images eliminated artifacts due to noise from the detector. To help eliminate ring artifacts caused by the detector elements, a random vertical movement of 5 was included. The projection radiographs were 16-bit TIFF files with 1048 x 2000 pixels.

A reconstruction algorithm (NRecon 1.1.4, Micro Photonics, Allentown, PA) digitally stacked and aligned these 2-D slices, resulting in a 3-D model of the sample which was used to analyse the two and three-dimensional morphological parameters of the defect. Quantitative analysis was based on the different attenuations of bone and soft tissue due to their different densities and compositions. Each volume element, or voxel (25 µm resolution), was assigned a grayscale value that was a threshold (Amira 5.0, Visualization Sciences, Burlington, MA). Bone volume fraction was calculated as bone pixels divided by total defect pixels.

VIII Histology

Freshly isolated samples were exposed under an UV fluorescent flashlight and photographed to analyse cell engraftment (Figure 6). Following imaging, samples were fixed in 10% neutral buffered formalin (Fisher Scientific, Fair Lawn, NJ) for two weeks, dehydrated in an ethanol series (70, 80, 90, and 100%) and infiltrated with methyl methacrylate (MMA, Acros Organics, Geel, Belgium) liquid monomer. Poly-methyl methacrylate (PMMA, Polysciences, Warrington, PA) solid beads and benzoyl peroxide (Sigma 33581) were added to induce polymerization and embed the samples. Samples were then sectioned perpendicular to the long axis of the cylindrical defect using a Buehler Isomet 100 diamond saw (Lake Bluff, IL) to yield 500 µm thick sections. Sections were polished to 300 µm thickness with increasing grades of zirconium sandpaper. Three sections, one in the center and two at opposing edges, were analysed.

Sections were stained with Sanderson's Rapid Bone Stain (Dorn & Hart Microedge, Villa Park, IL) and counterstained with acid fuchsin (Sigma F8129) to differentiate calcification (red) from soft callus (blue) and scar tissue (unstained). A digital scanner (HP Deskjet F4400, Miami, FL) captured images at full scale for quantification using image analysis software (ImageJ, National Institutes of Health, Bethesda, MA). The

mineralized bone area was calculated as the area of tissue staining positively for bone (purple) per total defect area.

IX Statistical Analysis

Quantitative data are presented as mean ± standard error. One-way analysis of variance (ANOVA) was performed using SAS 9.2 statistical analysis software (SAS Institute, Cary, NC). Fisher's exact test was used for pairwise mean comparisons. A total of 6 defects per treatment (n = 6) were analysed for a total of 24 defects. Statistical significance was evaluated using an alpha value of 0.05.

Results

In a preliminary experiment, we evaluated the number of ASCs encapsulated in fibrin and PRP; the results showed no statistically significant difference (p= 0.25). After eight weeks post-surgery, the mandibles were collected and analysed by CT-scan. In the images obtained (Figure 1), it is possible to evaluate the closing of the defects, the level of healing of the defects in the ramus. Secondly, we went on to evaluate the bone mineral density of the defect (Figure 2) and relative change in BMD compared to the original drilled bone (Figure 3).

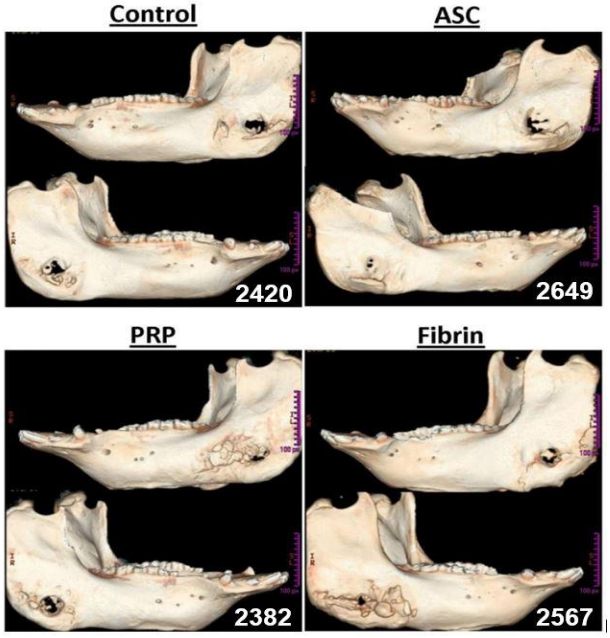

Figure 1: Representative computed tomography (CT) scans of whole mandibles with critical size defects. White pixels indicate high bone mineral density while black pixels indicate low density.

The results showed a higher BMD value in the ASC alone treatment, which is statistically different when compared with the control treatment (p = 0.032). The other groups (platelet-rich plasma p = 0.028; fibrin p = 0.036) also had statistically higher BMD when compared to the control treatment. When we evaluated the BMD, we found statistical differences between all groups containing ASC when compared with the control. In addition, the fibrin group had a higher BMD when compared with the ASC-only group (p = 0.041). The bone volume fraction (Figure 4) in the defect was higher for the ASC (p = 0.0039), PRP (p = 0.0011), and fibrin (p = 0.0035) treatments compared to controls (Figure 5). Furthermore, the bone volume fraction of both the PRP (p = 0.044) and the fibrin (p = 0.016) treatments was significantly higher when compared to ASC-only injections.

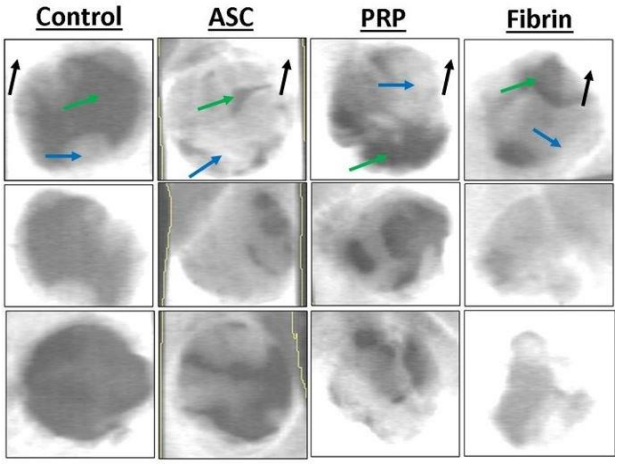

Figure 2: Representative dual energy X-ray absorptiometry (DXA) scans of critical size defects of various treatments. White pixels indicate high bone mineral density, grey is intermediate, while black pixels indicate low density. Mature cortical bone is indicated by black arrows. Immature woven bone from regeneration in the defect is indicated by blue arrows. Soft tissue is indicated by green arrows.

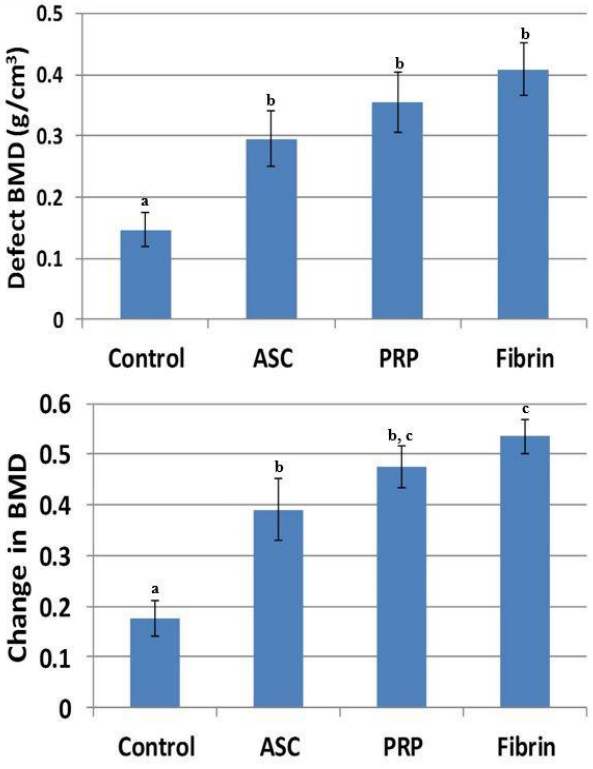

Figure 3. Bone mineral density of the defect (top) and relative change in BMD compared original drilled bone (bottom). BMD was significantly higher for all three treatments using ASCs. Relative change in BMD was significantly higher for fibrin compared to ASC-only. Treatments with different superscripts significantly differ ($p < 0.05$).

Finally, to verify the presence of the stem cells injected, we went on to evaluate the presence of GFP cells. Representative fluorescent images of bone defects injected with GFP tracer ASCs (1 million cells per defect) displayed areas of green color representing potential cell

engraftment within healing bone tissue (Figure 6). However, individual cells could not be located using confocal microscopy.

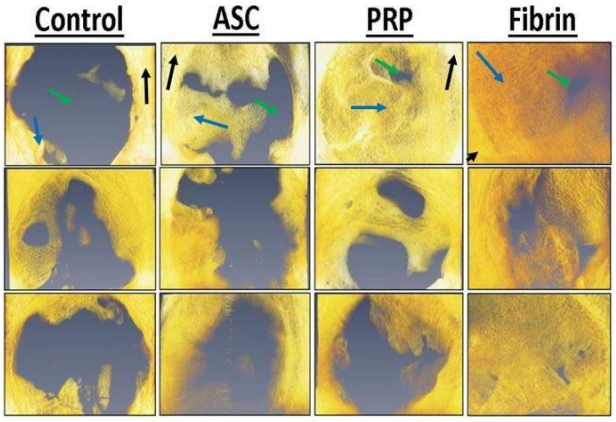

Figure 4: Representative micro-computed tomography reconstructions of bone defects of various treatments. Yellow/orange pixels represent mineralized tissue and grey pixels indicate soft tissue. Mature cortical bone is indicated by black arrows. Immature woven bone from regeneration in the defect is indicated by blue arrows. Soft tissue is indicated by green arrows.

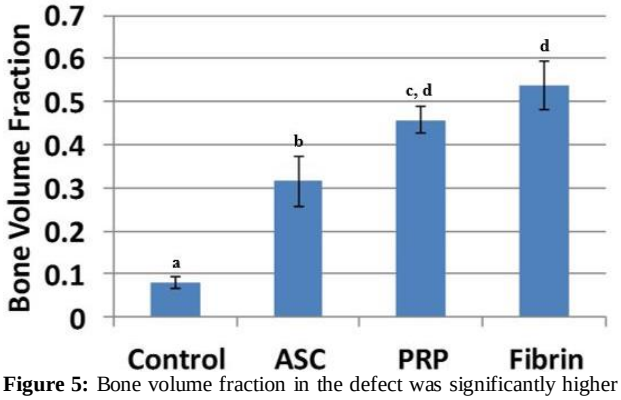

Figure 5: Bone volume fraction in the defect was significantly higher for all three cell treatments compared to controls. Bone volume fraction of both PRP and fibrin was significantly higher compared to ASC-only injections. Treatments with different superscripts significantly differ ($p < 0.05$).

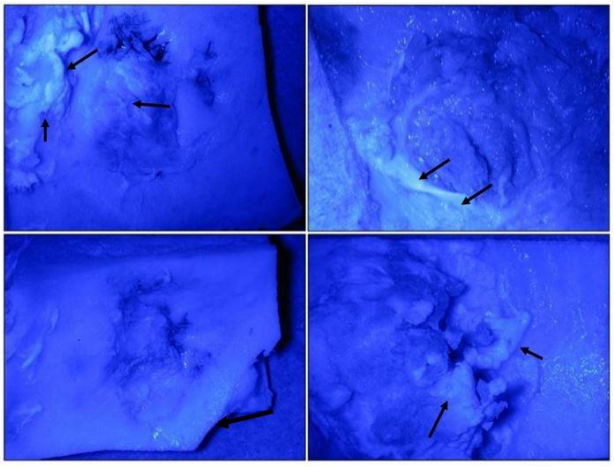

Figure 6: Representative fluorescent images of bone defects injected with GFP tracer ASCs. Areas of green colour (black arrows) represent potential cell engraftment within healing bone tissue. However, individual cells could not be located using confocal microscopy.

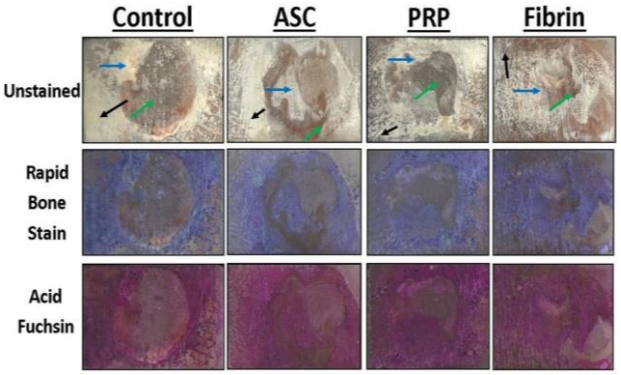

Figure 7: Representative histological sections of the porcine mandible containing the critical-size defect with different stains. Portions of mineralized bone in unstained sections appear white and soft tissue and scar tissue is yellow in color. Organized collagen in bone stains blue with Sanderson's Rapid Bone Stain while scar tissue is unstained. Mineralized tissue stains red with acid fuchsin counterstaining. Mineralized bone stains blue with Rapid Bone Stain and red with acid fuchsin and appears purple in color. Mature cortical bone is indicated by black arrows. Immature woven bone from regeneration within the defect is indicated by blue arrows. Soft tissue is indicated by green arrows.

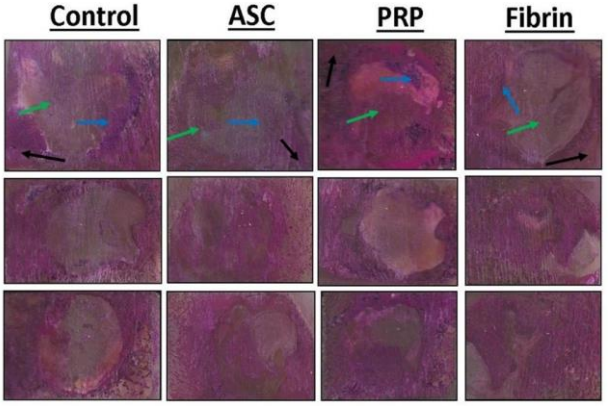

Figure 8: Representative histological sections of the porcine mandible containing the critical-size defect. Organized collagen in bone stains blue with Sanderson's Rapid Bone Stain while scar tissue is unstained. Mineralized tissue stains red with acid fuchsin counterstaining. Mineralized bone stains blue with Rapid Bone Stain and red with acid fuchsin and appears purple in color. Mature cortical bone is indicated by black arrows. Immature woven bone from regeneration within the defect is indicated by blue arrows. Soft tissue is indicated by green arrows.

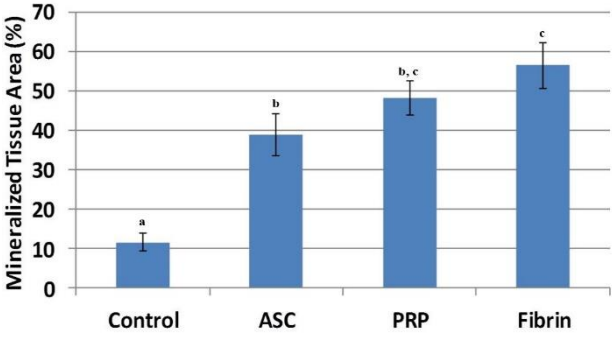

Figure 9: Mineralized tissue area in the defect was significantly higher for all three cell treatments compared to controls. Mineralized tissue area of fibrin was significantly higher compared to ASC-only injections. Treatments with different superscripts significantly differ ($p < 0.05$).

Portions of mineralized bone in unstained sections appeared white while soft tissue and scar tissue appeared yellow in color. Organized collagen in bone stains blue with Sanderson's Rapid Bone Stain while scar tissue is unstained (Figure 7). Mineralized tissue stains red with acid fuchsin counterstaining (Figure 8).

Mineralized tissue area in the defect was significantly higher for ASC ($p = 0.0037$), PRP ($p = 0.0015$), and fibrin ($p = 0.010$) treatments compared to controls (Figure 9). The mineralized tissue area of fibrin treatment was also significantly higher when compared to ASC-only injections ($p = 0.048$).

Discussion

The objective of this porcine animal model experiment was to compare autologous therapeutic options using adipose-derived stem cells alone, ASCs supplemented with platelet-rich plasma, and ASCs encapsulated in fibrin scaffolds derived from whole blood in terms of new bone formation after 8 weeks. Based on the results, autologous ASCs encapsulated in fibrin supplemented with calcium hydrogen phosphate were determined to be the treatment that resulted in the most bone formation of those tested, while platelet-rich plasma treatment resulted in only a slight reduction in bone volume fraction ($p = 0.25$). These supplements to ASCs significantly increased bone volume fraction compared to ASCs alone ($p < 0.044$), indicating the potential for improvement in adult stem cell therapies for bone defects.

The positive results of this study and others may, in part, be explained by the critical-size defect model employed [22, 27, 28]. Our mandibular ramus model (Figure 2) maintains several advantages, including non-weight bearing defects, quantitative analysis, reproducibility, and minimal changes to animal care. However, this model also has conditions favorable toward bone growth independent of treatment, including mechanical stabilization, defined bony edges with complete debridement, intactness of periosteum, and cyclical biomechanical loading due to mastication [29-31]. In addition, while the animals analysed were sexually and skeletally mature, the pigs were relatively young and in good health [14, 32]. Despite these model advantages, vehicle controls treated with only DMEM resulted in bone volume fraction recovery of less than 10%, suggesting that the 25 mm defects being utilized are critical-size defects.

Administration of autologous ASCs aided in the healing of this critical-size defect that would continue to heal and remodel spontaneously, resulting in more than 3-fold improvement in bone formation compared to controls (Figures 4, 7). The mechanism of healing is likely closely related to the limitations of regeneration and the production of scar tissue of a critical-size defect. Simultaneous factors such as insufficient signaling molecules, neovascularization, or MSC recruitment may all play a role in the limited regenerative response during a critical-size defect [33]. As a heterogeneous mixture of fibroblasts, endothelial cells, smooth muscle cells, and other cell types, ASCs have the potential to alleviate each of these limitations through the release of growth factors, the formation of new blood vessels, and further recruitment of regenerative cells to the site of the defect. Though not definitive, the apparent location of GFP from tracer ASCs injected at the defect site (Figure 6) would suggest that these cells are capable of differentiation and engraftment into newly forming tissue.

However, one potential problem limiting the therapeutic success of ASC administration may be the lack of cell encapsulation at the site of the defect if only a liquid vehicle is used. Cell encapsulation constricts cells and prevents their potential migration to sites other than the defect, reducing dilution of cell concentrations as well as the theoretical risk of tumor formation at ectopic sites [34]. Furthermore, bone has the increased potential to form in the center of the defect in addition to the edges, allowing healing to proceed more rapidly in multiple directions, eventually capable of forming bridges. Geometrically, bone formation at multiple sites serves to functionally reduce defect spaces and increase the size by which healing becomes critically limited. Therefore, due to differences in the ability to encapsulate cells at the concentrations tested, the comparison between PRP and fibrin is imperfect, as ASCs were not viable at concentrations where PRP formed a stable gel (above 50%). Better cell encapsulation using fibrin likely explains the moderate improvement in bone formation of fibrin compared to PRP treatments.

Differences in radiographic methods used in the study were noted. Dual energy X-ray absorptiometry (Figure 3) is two-dimensional method dependent, in part, on the thickness of the bone sample, which varied in the pig mandibles analysed, resulting in variation in bone mineral density values. Accounting for this thickness variation by normalization by the original, surgically removed bone reduced this discrepancy and likely improved precision of the measurement. In comparison, the three-dimensional method of micro-computed tomography (Figure 5) takes thickness into account and appears to be a more precise method for the circular ramus defect model. Based on measurements of bone mineral density and volume fraction, average bone mineral mass produced in the defect was estimated to range from 0.235 g for controls, 1.76 g for ASCs, 3.09 g for PRP, and 4.08 g for fibrin. Only 9.3 mg of calcium phosphate was added to fibrin scaffolds, so the contribution of exogenous $CaHPO_4$ towards the bone mineral density measurement was likely to be less than 1%. While DXA and micro-CT have different precisions using this model, both provide useful information regarding the degree of bone healing in the cylindrical defect, and the results are in general agreement.

The approach of using fibrin scaffolds or platelet-rich plasma has several advantages, including rapid clinical translation, a low risk-benefit ratio, and effective improvement in bone formation. Nearly all materials in this prospective therapy are already approved by the Food and Drug Administration for clinical use. The use of autologous materials decreases the risk of immune rejection, microbial contamination, and disease transmission, often associated with currently employed autograft methods. In addition, the inexpensive collection and processing of cells in this proposed treatment could significantly decrease treatment costs.

Both fibrin and PRP treatments have minor drawbacks. The drawing of non-clotted blood requires rapid processing and increases the risk of syringe blockage. Excess fibrin has also been associated with the formation of scar tissue, some of which was observed during sample collection [35-38]. In the craniofacial region, this scar tissue may result in reduced patient satisfaction. In the case of PRP, the pro-inflammatory component of the released platelet factors results in more pain and swelling than a standard surgery for several days post-surgery. This additional swelling may require thicker, stronger sutures to stay within breaking strength, which may result in larger scars at the incision site. Generally, the benefits of improved bone formation in these treatments derived from autologous sources may be worth the risks posed.

Future work to improve these autologous therapies may include the substitution of autologous bone dust/chips, or nano-calcium sulfate in place of calcium phosphate [39, 40]. Besides being a more autologous approach, bone chips harvested during the surgical removal of bone maintain lacunae, which house osteocytes that remain viable if collected and re-implanted within the timeframe of a standard bone graft surgery. Furthermore, bone chips contain remnants of trabecular architecture capable of infiltration by newly forming blood vessels, compared to calcium phosphate granules that are generally internally solid and impenetrable. Improvements in PRP processing to improve ASC viability at higher concentrations may improve bone formation, as the biological adhesive properties of gelled PRP may improve bone grafting. Osmotic balancing along with fine-tuning of anticoagulant: calcium ratios may result in cell viability suitable for ASC administration. Further studies using more clinically-relevant bone defects, such as calvarial, mandibular segmental, or femoral traction defects, among others, or using pigs in states of compromised bone healing, such as diabetes or older in age, are warranted [41-46]. Because the autologous materials studied in this study cannot bear significant loads, a much stiffer scaffold and/or other methods of stabilization would be required for body weight-bearing applications.

We conclude that the addition of autologous blood products, either 20% platelet-rich plasma or fibrin scaffolds derived from whole blood supplemented with calcium phosphate, to adipose-derived stem cells derived from lipoaspirate, may be advantageous due to improved bone formation without requiring harvesting of patient bone. In summary, the present study demonstrates the potential for improvement in cell therapies towards an autologous bone tissue construct for craniofacial bone repair.

Acknowledgements

The authors would like to thank Molly Sermersheim (University of Illinois) for help with editing of the manuscript. The authors would also like to thank and dedicate this manuscript to Dr. Michael S. Goldwasser (Chapel Hill, NC and Urbana, IL) for his inspiration, his critical thinking regarding craniofacial regeneration and his devotion to countless patients over many years.

Conflicts of Interest

None.

Funding

A portion of the work presented here was partially supported by the Carle Foundation Hospital (#2007–04072), Urbana, IL and the Illinois Regenerative Medicine Institute (IDPH Grant # 63080017).

Ethical Approval

All procedures performed in studies involving animals were in accordance with the ethical standards of the University of Illinois Institutional Animal Care and Use Committee, (IACUC Approval # 10014). This article does not contain any studies with human participants performed by any of the authors.

Abbreviation

2-D: Two Dimensional
3-D: Three Dimensional
ASCs: Adipose Stem Cells
ANOVA: One-Way Analysis Of Variance
BMD: Bone Mineral Density
CT: Computed Tomography
DAPI: 4′,6-Diamidino-2-Phenylindole
DMEM: Dulbecco's Minimal Essential Medium
DXA: Dual Energy X-Ray Absorptiometry
GFP-ASCs: Green Fluorescent Protein Labelled Adipose Stem Cells
kPa: kilopascal
kV: kilovolt
MMA: Methyl methacrylate
MicroCT: Micro Computed Tomography
mA: miliamperes
PBS: Phosphate- Buffered Saline
PRP: Autologous Platelet-Rich Plasma
PMMA: Poly-Methyl methacrylate
RBCs: Red Blood Cells
TIFF: Tagged Image File Format
UV: Ultraviolet

REFERENCES

1. Panagiotis Megas (2005) Classification of non-union. *Injury* 36: S30-S37. [Crossref]
2. Romesh P Nalliah, Veeratrishul Allareddy, Min Kyeong Kim, Shankar R Venugopalan, Praveenkumar Gajendrareddy et al. (2013) Economics of facial fracture reductions in the United States over 12 months. *Dent Traumatol* 29: 115-120. [Crossref]
3. H R Cattermole, J R Hardy, P J Gregg (1996) The footballer's fracture. *Br J Sports Med* 30: 171-175. [Crossref]
4. Holmes D (2017) Non-union bone fracture: a quicker fix. *Nature* 550: S193. [Crossref]
5. U Kneser, D J Schaefer, E Polykandriotis, R E Horch (2006) Tissue engineering of bone: the reconstructive surgeon's point of view. *J Cell Mol Med* 10: 7-19. [Crossref]
6. Jingtao Zhang, Weizhen Liu, Verena Schnitzler, Franck Tancret, Jean-Michel Bouler (2014) Calcium phosphate cements for bone substitution: chemistry, handling and mechanical properties. *Acta biomaterialia* 10: 1035-1049. [Crossref]
7. Moore WR, Graves SE, Bain GI (2001) Synthetic bone graft substitutes. *ANZ J Surg* 71: 354-361. [Crossref]
8. Langer R, Vacanti JP (1993) Tissue engineering. *Science* 260: 920-926. [Crossref]
9. Gestring GF, Lerner R (1983) Autologous Fibrinogen for Tissue-Adhesion, Hemostasis and Embolization. *Vascular Surg* 17: 294-304.
10. Silvestro Canonico (2003) The use of human fibrin glue in the surgical operations. *Acta Biomed* 74: 21-25. [Crossref]
11. William D Spotnitz, Roshan Prabhu (2005) Fibrin sealant tissue adhesive--review and update. *J Long Term Eff Med Implants* 15: 245-270. [Crossref]
12. Yanning Liu, Xi Yan, Zhao Sun, Bin Chen, Qin Han et al. (2007) Flk-1+ adipose-derived mesenchymal stem cells differentiate into skeletal

muscle satellite cells and ameliorate muscular dystrophy in mdx mice. *Stem Cell Develop* 16: 695-706. [Crossref]

13. Rosa Yañez, María Luisa Lamana, Javier García-Castro, Isabel Colmenero, Manuel Ramírez et al. (2006) Adipose tissue-derived mesenchymal stem cells have in vivo immunosuppressive properties applicable for the control of the graft-versus-host disease. *Stem cells* 24: 2582-2591. [Crossref]
14. Shanna M Wilson, Michael S Goldwasser, Sherrie G Clark, Elisa Monaco, Massimo Bionaz et al. (2012) Adipose-derived mesenchymal stem cells enhance healing of mandibular defects in the ramus of swine. *J Oral Maxillofac Surg 70*: e193-e203. [Crossref]
15. Derek J Milner, Massimo Bionaz, Elisa Monaco, Jo Ann Cameron, Matthew B Wheeler (2018) Myogenic potential of mesenchymal stem cells isolated from porcine adipose tissue. *Cell Tissue Res* 372: 507-522. [Crossref]
16. Gail E Kilroy, Sandra J Foster, Xiying Wu, Joseph Ruiz, Sonya Sherwood et al. (2007) Cytokine profile of human adipose-derived stem cells: expression of angiogenic, hematopoietic, and pro-inflammatory factors. *J cell physiol* 212: 702-709. [Crossref]
17. Marcello Rubessa, Kathryn Polkoff , Massimo Bionaz, Elisa Monaco, Derek J Milner et al. (2017) Use of Pig as a Model for Mesenchymal Stem Cell Therapies for Bone Regeneration. *Animal biotechnol* 28: 275-287. [Crossref]
18. E Monaco, M Bionaz, S J Hollister, M B Wheeler (2011) Strategies for regeneration of the bone using porcine adult adipose-derived mesenchymal stem cells. *Theriogenology* 75: 1381-1399. [Crossref]
19. Massimo Bionaz, Elisa Monaco, Matthew B Wheeler (2015) Transcription Adaptation during In Vitro Adipogenesis and Osteogenesis of Porcine Mesenchymal Stem Cells: Dynamics of Pathways, Biological Processes, Up-Stream Regulators, and Gene Networks. *PLoS One* 10: e0137644. [Crossref]
20. Christopher M Runyan, Donna C Jones, Kevin E Bove, Rian A Maercks, David S Simpson et al. (2010) Porcine allograft mandible revitalization using autologous adipose-derived stem cells, bone morphogenetic protein-2, and periosteum. *Plast Reconstr Surg* 125: 1372-1382. [Crossref]
21. P A Zuk, M Zhu, H Mizuno, J Huang, J W Futrell et al. (2001) Multilineage cells from human adipose tissue: implications for cell-based therapies. *Tissue Eng* 7: 211-228. [Crossref]
22. Daniel W Weisgerber, Derek J Milner, Heather Lopez-Lake, Marcello Rubessa, Sammi Lotti et al. (2018) A Mineralized Collagen-Polycaprolactone Composite Promotes Healing of a Porcine Mandibular Defect. *Tissue Eng Part A* 24: 943-954. [Crossref]
23. Elizaveta Kon, Giuseppe Filardo, Marco Delcogliano, Mirco Lo Presti, Alessandro Russo et al. (2009) Platelet-rich plasma: new clinical application: a pilot study for treatment of jumper's knee. *Injury* 40: 598-603. [Crossref]
24. Flinn Shiel, Carl Persson, James Furness, Vini Simas, Rodney Pope et al. (2018) Dual energy X-ray absorptiometry positioning protocols in assessing body composition: A systematic review of the literature. *J sci med sport* 21: 1038-1044. [Crossref]
25. Sheeny K Lan Levengood, Samantha J Polak, Michael J Poellmann, David J Hoelzle, Aaron J Maki et al. (2010) The effect of BMP-2 on micro- and macroscale osteointegration of biphasic calcium phosphate scaffolds with multiscale porosity. *Acta biomaterialia* 6: 3283-3291. [Crossref]
26. Dewey MJ, Johnson EM, Slater ST, Milner DJ, Wheeler MB et al. (2020) Mineralized collagen scaffolds fabricated with amniotic membrane matrix increase osteogenesis under inflammatory conditions. *Regenerat Biomaterial* 2020.
27. Jeffrey M Gimble, Warren Grayson, Farshid Guilak, Mandi J Lopez, Gordana Vunjak-Novakovic (2011) Adipose tissue as a stem cell source for musculoskeletal regeneration. *Front Biosci (Schol Ed)* 3: 69-81. [Crossref]
28. Kevin C Hicok, Tracey V Du Laney, Yang Sheng Zhou, Yuan-Di C Halvorsen, Daron C Hittet al. (2004) Human adipose-derived adult stem cells produce osteoid *in vivo*. *Tissue Eng* 10: 371-380. [Crossref]
29. Hiltunen A, Vuorio E, Aro HT (1993) A standardized experimental fracture in the mouse tibia. *J Orthopaed Res* 11: 305-312. [Crossref]
30. Ozaki A, Tsunoda M, Kinoshita S, Saura R (2000) Role of fracture hematoma and periosteum during fracture healing in rats: interaction of fracture hematoma and the periosteum in the initial step of the healing process. *J orthopaed sci* 5: 64-70. [Crossref]
31. H T Aro, E Y Chao (1993) Bone-healing patterns affected by loading, fracture fragment stability, fracture type, and fracture site compression. *Clin Orthopaed Relat Res* 293: 8-17. [Crossref]
32. B R White, Y H Lan, F K McKeith, J Novakofski, M B Wheeler et al. (1995) Growth and body composition of Meishan and Yorkshire barrows and gilts. *J Animal Sci* 73: 738-749. [Crossref]
33. Frédéric Deschaseaux, Luc Sensébé, Dominique Heymann (2009) Mechanisms of bone repair and regeneration. *Trend Mol Med* 15: 417-429. [Crossref]
34. Yu JM, Jun ES, Bae YC, Jung JS (2008) Mesenchymal stem cells derived from human adipose tissues favor tumor cell growth in vivo. *Stem cell Dev* 17: 463-473. [Crossref]
35. K Overgaard, T Sereghy, G Boysen, H Pedersen, S Høyer, N H Diemer (1992) A rat model of reproducible cerebral infarction using thrombotic blood-clot emboli. *J Cereb Blood Flow Metab* 12: 484-490. [Crossref]
36. Staindl O (1979) The healing of wounds and scar formation under the influence of a tissue adhesion system with fibrinogen, thrombin, and coagulation factor XIII. *Arch Otorhinolaryngol* 222: 241-245. [Crossref]
37. Allan Fernando Giovanini, Carla Castiglia Gonzaga, João Cesar Zielak, Tatiana Miranda Deliberador, Juliane Kuczera et al. (2011) Platelet-rich plasma (PRP) impairs the craniofacial bone repair associated with its elevated TGF-beta levels and modulates the co-expression between collagen III and alpha-smooth muscle actin. *J Orthop Res* 29: 457-463. [Crossref]
38. Por YC, Barcelo CR, Salyer KE, Genecov DG, Troxel K et al. (2008) Bone generation in the reconstruction of a critical size calvarial defect in an experimental model. *J Craniofac Surg* 19: 383-392.
39. Zunpeng Liu, Xue Yuan, Gabriela Fernandes, Rosemary Dziak, Ciprian N Ionita et al. (2017) The combination of nano-calcium sulfate/platelet rich plasma gel scaffold with BMP2 gene-modified mesenchymal stem cells promotes bone regeneration in rat critical-sized calvarial defects. *Stem Cell Res Ther* 8: 122. [Crossref]
40. Tayapongsak P, O'Brien DA, Monteiro CB, Arceo-Diaz LY (1994) Autologous fibrin adhesive in mandibular reconstruction with particulate cancellous bone and marrow. *J oral maxillofacial surg* 52: 161-165. [Crossref]
41. Han Tsung Liao, Ming-Jin Tsai, Manuri Brahmayya, Jyh-Ping Chen (2018) Bone Regeneration Using Adipose-Derived Stem Cells in Injectable Thermo-Gelling Hydrogel Scaffold Containing Platelet-Rich Plasma and Biphasic Calcium Phosphate. *Int J Mol Sci* 19: 2537. [Crossref]

42. Haisong Xu, Ke Ke, Zhiliang Zhang, Xuan Luo, Xin Jin et al. (2013) Effects of platelet-rich plasma and recombinant human bone morphogenetic protein-2 on suture distraction osteogenesis. *J craniofacial surg* 24: 645-650. [Crossref]
43. Bou Assi T, Rahme M, Saghieh S, Bou Raad Azoury N, Abdallah Hajj Hussein I et al. (2013) Effect of autologous platelet-rich plasma on distraction osteogenesis in the mandible of rabbits: a morphologic and morphometric approach. *J Biol Regul Homeost Agents* 27:177-187. [Crossref]
44. C Bosch, B Melsen, K Vargervik (1998) Importance of the critical-size bone defect in testing bone-regenerating materials. *J Craniofacial Surg* 9: 310-316. [Crossref]
45. Schmitz JP, Hollinger JO (1986) The critical size defect as an experimental model for craniomandibulofacial nonunions. *Clin Orthop Relat Res* 1986: 299-308. [Crossref]
46. Harold Brem, Marjana Tomic-Canic (2007) Cellular and molecular basis of wound healing in diabetes. *J Clin Invest* 117: 1219-1222. [Crossref]